Completeness of the exact muffin-tin orbitals: Application to hydrogenated alloys

N. I. Al-Zoubi,[1,2] M. P. J. Punkkinen,[1] B. Johansson,[1,3] and L. Vitos[1,3,4]
[1]*Applied Materials Physics, Department of Materials Science and Engineering, Royal Institute of Technology, SE-100 44 Stockholm, Sweden*
[2]*Department of Applied Material Physics, Tafila Technical University, Tafila, Jordan*
[3]*Division for Materials Theory, Department of Physics and Materials Science, Uppsala University, SE-75121 Uppsala, Sweden*
[4]*Research Institute for Solid State Physics and Optics, P.O. Box 49, H-1525 Budapest, Hungary*
(Received 25 September 2009; revised manuscript received 17 December 2009; published 22 January 2010)

We investigate the basis set convergence of the exact muffin-tin orbitals by monitoring the equation of state for Al, Cu, and Rh calculated in the conventional face-centered-cubic lattice (str-I) and in a face-centered-cubic lattice with one atomic and three empty sites per primitive cell (str-II). We demonstrate that three (*spd*) muffin-tin orbitals are sufficient to describe Al in both structures, but for str-II Cu and Rh at least five (*spdfg*) orbitals are needed to get converged equilibrium Wigner-Seitz radius (within $\lesssim 0.8\%$) and bulk modulus ($\lesssim 3.3\%$). We ascribe this slow convergence to the nearly spherical densities localized around the Cu and Rh atoms, which create strongly asymmetric charge distributions within the nearest cells around the empty sites. The potential sphere radius dependence of the theoretical results for structure str-II is discussed. It is shown that a properly optimized overlapping muffin-tin potential in combination with the *spdfg* basis yields acceptable errors in the equilibrium bulk properties. The basis set convergence is also shown on hydrogenated Sc and Sc-based alloys.

DOI: 10.1103/PhysRevB.81.045122 PACS number(s): 71.15.Ap, 71.15.Nc, 61.50.Lt

I. INTRODUCTION

An important group of density-functional methods[1] is built around the so-called muffin-tin (MT) approximation. The approximation originates from the observation that the exact crystal potential is atomiclike around the lattice sites (where the core states are located) and nearly flat between the atoms. Accordingly, within the MT approximation one substitutes the Kohn-Sham effective potential[2] by spherically symmetric potentials centered on atoms plus a constant potential in the interstitial region. The MT family includes the standard Korringa-Kohn-Rostoker (KKR) (Refs. 3 and 4) and screened-KKR (Ref. 5) methods, methods based on the atomic sphere approximation (ASA) (Refs. 6–9) as well as the recently developed exact muffin-tin orbital (EMTO) formalism.[10–15] The full-potential generalizations of the MT types of methods, e.g., the full-potential linear muffin-tin orbital (LMTO) methods[16–18] or the full-potential KKR method,[19] are excluded from the above MT group since in principle they are free of any shape approximation.

The MT methods have been used for a long time in the *ab initio* description of the electronic structure of crystalline solids. Often, the output electron density was used to calculate the total energy of solids. For instance, standard MT methods were suitable to compute the equation of state of metals with sufficient high accuracy.[20,21] However, since in these applications the shape approximation was adopted also to the charge density (only a spherical density was included) and total energy, it turned out that these early MT implementations were restricted to densely packed solids. Several measures have been taken to extend the MT approach to open or distorted lattices. The combined correction,[7] the electrostatic or Madelung correction,[22] and the kinetic-energy correction[23] were common means for improving the accuracy of the MT methods. A truly front-breaking step, however, was computing the full-charge density (FCD) from the output of a self-consistent MT calculation and using that density to calculate the total energy.[23,24] Originally, the FCD technique was exclusively combined with the LMTO method.[6,7] However, the LMTO-FCD approach was still lacking an accurate kinetic-energy term, which limited its application to systems with high crystal symmetry. Some years ago, the FCD technique was implemented within the EMTO formalism, which led to a highly accurate and efficient MT total-energy method.[12] This approach, in combination with the coherent potential approximation,[14,15] has become a successful and widely used tool in the theoretical study of the thermophysical properties of metallic alloys[13,15,25–36] and complex oxides.[37–40]

The strength of the MT methods is their high efficiency compared to the all-electron full-potential methods. This may, first of all, be ascribed to the spherical approximation to the Kohn-Sham effective potential. In most of the MT implementations, the Poisson's equation is solved for the spherical potential using spherical cells around the lattice sites. Another important characteristic of the MT methods is the employed minimal basis set. The MT orbitals are constructed from the partial waves (solutions of the Schrödinger equation for the spherical potential) within the muffin-tin spheres and the Bessel and Neumann functions (solutions of the Helmholtz equation for the constant potential) in between the spheres. The number of orbitals is set by the maximum orbital quantum number (l_{max}), which is also the cutoff adopted for the tail functions entering via the two-center expansion of the envelope (Neumann) functions. Therefore, l_{max} is the key parameter for the completeness of the basis set and thus has an important effect on the accuracy of the method.

In MT methods, typically three to four orbitals per site were found to be sufficient to compute with a high accuracy the one-electron energies and wave functions of metals with close-packed crystal lattice. Using *spd* orbitals ($l_{max}=2$) within the LMTO-ASA method provided a reliable descrip-

tion of the crystal structure of simple and transition metals.[22] Nevertheless, when the spherical symmetric approximation for the charge density was partially lifted (e.g., by including the dipole density moments) it turned out that *f* states must also be taken into account in order to improve the agreement between MT and full-potential methods[23,41] and sometimes even to produce meaningful results.[42] Then one may ask what is the proper basis set in an FCD calculation, where no shape constraint is employed for the density. The question becomes especially important when the MT method is applied to systems where the potential and the density strongly violate the MT picture.

The object of this work is to give a detailed answer to the above problem. To this end, we investigate the basis set convergence of the muffin-tin orbitals using the EMTO approach in combination with the FCD scheme. We demonstrate that the number of orbitals needed for converged equilibrium bulk properties strongly depends on the actual geometry and potential. Close-packed structures and simple metals are well described by the *spd* or *spdf* basis. On the other hand, open structures and nonspherical potentials require a significantly larger basis set. In particular, transition metals with semicore states located close to the valance band show surprisingly slow basis convergence.

The EMTO formalism is based on the optimized overlapping muffin-tin (OOMT) potential approach, where the radii of the potential spheres are treated as variables.[13,15,43] Therefore, by employing the EMTO method for the present study, in addition to the basis set, we have the opportunity to investigate how the size of the overlapping MT potential spheres influences the accuracy of the calculated physical properties. The results presented here caution the EMTO practitioners to pay special attention when setting up these spheres since they affect the optimized muffin-tin potential and by that also the total energy and thus all derived quantities.

The rest of the paper is divided in three main sections. In Sec. II, we introduce the computational tool, define the systems for which the test calculations are carried out, and give important numerical details of the calculations. Results of the test calculations are presented and discussed in Sec. III. As an application of the present methodological developments, in Sec. IV we study the hydrogen reaction with Sc and Sc-based alloys.

II. METHODOLOGY

A. Computational method

The present study is based on the exact muffin-tin orbital method[10–15] in combination with the full-charge density technique.[23,24] The EMTO method is an improved screened KKR method, where the Kohn-Sham equations are solved for the so-called OOMT potential. More details about the EMTO theory and its implementation are given in Refs. 10 and 15.

The philosophy behind the OOMT potential is to find the best overlapping MT approximation to the full potential. Comparing the early results obtained using a nonoverlapping MT approach to those from an ASA calculation suggested that the overlapping ASA spheres describe more accurately the effective one-electron potential than the traditional MT approach. Later, it was shown that increasing the size of the potential spheres improves the accuracy of the muffin-tin approximation.[11,13] These findings motivated Andersen and co-workers to introduce the concept of optimized overlapping MT potentials.[11,43] The first step in designing the OOMT potential is to determine the spherical and the constant potentials by minimizing the mean of the squared deviation between the full potential and the overlapping MT potential. Details about the resulting integrodifferential equations and their solutions within the spherical cell approximation can be found in Refs. 15 and 43. Assuming that the OOMT potential is properly generated for fixed potential sphere radii, the next question is how to choose these radii in order to get the best representation of the full potential. In the standard implementation of the EMTO method,[13,15] a small error coming from the overlap of the potential spheres is neglected. With increasing sphere sizes, the error increases, which sets an upper limit for the linear overlap between the spheres and thus for the potential sphere radii. Therefore, in applications, one always needs to find the best potential sphere radii which already ensure a proper representation of the full potential but still lead to an acceptable overlap error in the total energy.

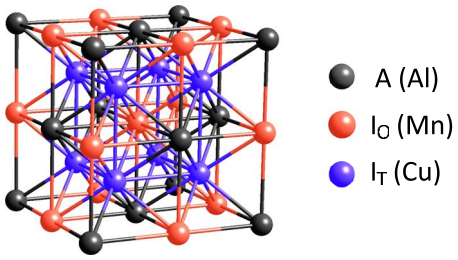

FIG. 1. (Color online) Schematic plot of the Heusler structure ($L2_1$, prototype $AlCu_2Mn$). In structure str-II, the black spheres (A) are the actual atoms, whereas the three interstitial sites, namely, the orange (I_O) octahedral site and the two blue (I_T) tetrahedral sites, are filled up with empty potential wells (Em).

B. Selecting the systems

Our aim is to select test systems where the local potentials and densities around the lattice sites are relatively far from the MT geometry. To this end, we start from the close-packed face-centered-cubic (fcc) parent lattice with one atom at (0,0,0). Next, we insert three interstitial sites per fcc primitive cell: one to the (1/2,1/2,1/2) octahedral position and two to the (1/4,1/4,1/4) and (3/4,3/4,3/4) tetrahedral positions (Fig. 1). The resulting lattice has a body-centered-cubic (bcc) packing and can be used as a prototype for a large variety of systems. For instance, when the fcc position is occupied by atom A (Ca), the tetrahedral positions by atom B (F), and the octahedral position is left empty (Em) we arrive to the fluorite (C1, CaF_2) structure. Atom A (Zn) on the fcc position, atom B (S) on the first tetrahedral positions, and empty second tetrahedral and octahedral positions give the zinc-blende (B3, ZnS) structure. The Heusler ($L2_1$, $AlCu_2Mn$) structure is recovered if the fcc position is occupied by atom A (Al), the

octahedral position by B (Mn), and the two tetrahedral positions by C (Cu). Placing similar atoms on the fcc and octahedral positions and leaving the tetrahedral positions empty result in a simple cubic structure, whereas filling up all four positions with similar atoms gives the bcc structure. Finally, partially or completely filled octahedral and tetrahedral positions are possible models for interstitials in an fcc host.

For the present tests, we consider the most inhomogeneous case when all interstitial sites from Fig. 1 are "occupied" by Em potential wells. By "empty potential well" we mean a potential well without atomic nucleus ($Z=0$) but presumably with a significant electronic charge. Using these Em sites, we can describe the fcc lattice as a Heusler type of lattice dressed up with one atomic and three Em potential wells. In the following, we refer to the original fcc lattice as str-I and to the dressed-up lattice as str-II.

Obviously, a properly performed full-potential calculation should yield identical total energies (and derived properties) for str-I and str-II. This is because in full-potential methods no shape approximation is used and thus the space division has no effect on the accuracy (apart from some controllable numerical problems). On the other hand, the description of the str-II system represents a real challenge for the MT methods. This can easily be foreseen if we realize that the tetrahedral Em wells in the str-II lattice are close to the (deep) spherical atomic potential wells located at the original fcc sites and thus both the potential and the charge density within these Em spheres will strongly deviate from the spherical symmetry. In other words, the muffin-tin character of the actual effective potential around the lattice sites, which has motivated the MT approximation, is strongly violated in structure str-II.

For the actual test calculations, we select Al, Cu, and Rh as three representative fcc metals having markedly different electronic structures and charge densities. Aluminum is a simple metal with delocalized electronic states. Copper, being a noble metal, has a more localized and nearly spherically symmetric charge density around the atomic sites. In rhodium, the semicore states are located relatively close to the valance band, which means that, depending on the size of the potential spheres, these states might penetrate into the Em spheres around the Rh atoms. To monitor the performance of the MT approach for structures str-I and str-II, we choose two fundamental quantities: the equilibrium Wigner-Seitz (WS) radius (w) and the bulk modulus (B). We pick these two parameters because (i) they should be the start-off for any well designed density-functional study and (ii) the EMTO method has proved a reliable tool for calculating the equation of state of fcc Al, Cu, and Rh.[15,44]

One may ask what is the point describing a simple fcc lattice as a complex dressed-up Heusler lattice with one atomic and three empty potential wells. Within muffin-tin (in fact all cellular) methods it is of basic importance to minimize the space-division dependence of the computed quantities. The total energy and derived properties (e.g., equation of state, elastic parameters, and phase stability) should not change significantly when introducing additional empty wells and repartitioning the unit cell by decreasing the size of the original Voronoi polyhedra and introducing new ones around the Em sites. In addition to these fundamental issues, a properly designed total-energy method should be able to describe partially or fully occupied interstitial sites within the close-packed systems. A good example for the partially occupied interstitial sites in the fcc lattice is the hydrogenated ScAlMg. Recent experimental studies[45] demonstrated that $ScAl_{0.8}Mg_{0.2}$ under 10 MPa hydrogen pressure transforms to ScH_2 plus $Al_{0.8}Mg_{0.2}$ around 400 °C. The hydrogenated sample heated under vacuum releases the hydrogen at ~500 °C. $ScAl_{0.8}Mg_{0.2}$ has the CsCl structure and ScH_2 adopts the fluorite (CaF_2) structure. Since ScH_2 is a particularly stable hydride, the observed hydrogen desorption around 500 °C has been ascribed[45] to the presence of Al and Mg, which significantly decrease the mixing free energy of hydrogen in $ScAl_{0.8}Mg_{0.2}$. In order to study the above chemical reaction using first principles, one should employ a computational tool which is suitable to (a) describe the interstitial sites in fcc lattice and (b) properly account for the chemical disorder between Al and Mg. In Sec. IV, we will show that both of these requirements are reasonably well handled by the EMTO method when a sufficiently large basis set is employed.

C. Numerical details

In the self-consistent EMTO calculations, the exchange-correlation term was described within the local-density approximation (LDA).[46,47] In addition to LDA, the total energy was also computed using the density functional by Perdew, Burke, and Ernzerhof (PBE) [48] and its recently revised version for solids and surfaces (PBEsol).[49] The gradient terms in these two approximations were included within the perturbative approach.[19] Namely, we used the total charge density obtained within LDA to compute the gradient-level total energies. This approach has been shown to produce errors which are within the numerical accuracy of our calculations.[44]

The one-electron equations were solved within the scalar-relativistic and soft-core approximations. The 3s states of Mg; the 3s and 3p states of Al; the 3d and 4s states of Cu; the 3d, 4s, and 3p states of Sc; and the 4d, 5s, and 4p states of Rh were treated as valance states. For Cu, we also performed an additional calculation by considering the 3p electrons as valance states, which will be referred to as Cu*. For all systems in structure str-I and for Al and Cu in structure str-II, the Green's function was calculated for 16 complex energy points distributed exponentially on a semicircular contour with radius of 0.5 Ry. For str-II Rh, Cu*, Sc, and ScAlMg, in order to include the semicore states within the contour, the radius of the contour was increased to 3 Ry and the number of energy points was increased to 61. Consequently, for these systems the EMTO slope matrix was generated using the two-center expansion as described in Ref. 50. In the basis set, we included orbitals up to $l_{max}=5$ ($spdfgh$) and the one-center expansion of the full-charge density was truncated at $l^h_{max}=8$.[15] To obtain the accuracy needed for the calculation of the equilibrium volume and bulk modulus, we used 240 uniformly distributed k points in the irreducible wedge of the fcc Brillouin zone.

The self-consistent calculations were performed within the spherical cell approximation.[13] According to that, the

TABLE I. Calculated equilibrium atomic radii (w^{I} in bohr) and bulk moduli (B^{I} in GPa) for fcc Al, Cu, and Rh as functions of the number of MT orbitals, l_{max}. Results are shown for LDA, PBE, and PBEsol exchange-correlation approximations.

	Al	Cu	Rh	Al	Cu	Rh	Al	Cu	Rh	Al	Cu	Rh
w^{I}		*spd*			*spdf*			*spdfg*			*spdfgh*	
LDA	2.95	2.62	2.82	2.95	2.60	2.78	2.95	2.60	2.78	2.95	2.60	2.78
PBE	2.99	2.70	2.88	2.99	2.69	2.84	2.99	2.68	2.83	2.99	2.68	2.83
PBEsol	2.97	2.65	2.84	2.97	2.64	2.80	2.97	2.63	2.80	2.97	2.63	2.80
B^{I}		*spd*			*spdf*			*spdfg*			*spdfgh*	
LDA	80.7	178.8	289.8	81.2	184.7	309.7	81.2	185.5	313.5	81.2	185.7	313.9
PBE	75.1	135.5	235.4	75.7	140.5	252.4	75.7	141.5	255.5	75.7	141.6	255.9
PBEsol	79.5	161.0	269.8	80.1	165.7	288.8	80.1	166.8	292.2	80.1	167.0	292.8

Wigner-Seitz cells (Voronoi polyhedra) around the lattice sites were approximated by spheres with radii equal to the average Wigner-Seitz radius: w^{I} for str-I and $\bar{w}^{\mathrm{II}}$ for str-II. Note that the average radius for str-I corresponds to $4^{1/3}$ times the average radius for str-II. In the following, for structure str-II we introduce a rescaled radius $w^{\mathrm{II}} \equiv 4^{1/3}\bar{w}^{\mathrm{II}}$, which can directly be compared to w^{I}. The Wigner-Seitz spheres around the lattice sites were kept fixed even when we changed the size of the potential spheres. For both structures, the equilibrium Wigner-Seitz radii (w^{I} and w^{II}) and the corresponding bulk moduli (B^{I} and B^{II}) were extracted from a Morse function[21] fitted to the total energies calculated for seven different volumes.

For structure str-I, the radius of the potential sphere (S) was always fixed to the average Wigner-Seitz radius, viz., $S^{\mathrm{I}}=1.00w^{\mathrm{I}}$. For structure str-II, $S^{\mathrm{II}}_{\mathrm{Em}}=1.00\bar{w}^{\mathrm{II}}$ was used for the three Em sites. For the atomic site A (A stands for Al, Cu, or Rh) we used three different radii: $S^{\mathrm{II}}_{\mathrm{A}}=1.00\bar{w}^{\mathrm{II}}$, $1.05\bar{w}^{\mathrm{II}}$, and $1.10\bar{w}^{\mathrm{II}}$. In this way, we were able to trace the effect of the size of the potential sphere on the theoretical equation of state for structure str-II.

III. RESULTS OF THE TEST CALCULATIONS

A. Structure str-I

The present theoretical equilibrium Wigner-Seitz radii and bulk moduli for fcc (str-I) Al, Cu, and Rh are listed in Table I as functions of l_{max} for three exchange-correlation approximations. For comparison, the room-temperature experimental w^{I} and B^{I} for Al, Cu, and Rh are 2.991, 2.669, and 2.803 bohr and 72.8, 133, and 282 GPa, respectively.[51] The EMTO results obtained for $l_{max}=3$ are in good agreement with our former theoretical values.[44] The small differences in the bulk modulus ($\lesssim 2\%$) are due to the different fitting procedures employed here and in Ref. 44. Because of that, we take 2% as being the error bar of our bulk modulus calculation. This error in B corresponds to $\sim 0.5\%$ (assuming $B' \approx 4$) uncertainty in the Wigner-Seitz radius.

Taking as the most accurate theoretical values those corresponding to *spdfgh*, from Table I we can establish the basis set convergence for structure str-I. As expected, for fcc Al already $l_{max}=2$ leads to well-converged w^{I} and B^{I}, whereas for fcc Cu and Rh $l_{max}=3$ is required to bring the errors of w^{I} and B^{I} down to 0.4% and 1.4%, respectively. Furthermore, we realize that the l_{max} dependence of w^{I} and B^{I} is very similar for LDA, PBE, and PBEsol, indicating that the gradient terms in PBE and PBEsol converge rapidly with the number of MT orbitals. Because of that, for structure str-II we present and discuss only the LDA results.

B. Structure str-II

1. Aluminum

Figure 2 shows the relative errors for the equilibrium Wigner-Seitz radius (δ_w) and bulk modulus (δ_B) of Al calculated for structure str-II as functions of l_{max} and $S^{\mathrm{II}}_{\mathrm{Al}}$. Numerical values are listed in Table II. The errors are defined as the relative deviations between $w^{\mathrm{II}}_{\mathrm{Al}}(l_{max}, S^{\mathrm{II}}_{\mathrm{Al}})$ and $w^{\mathrm{I}}_{\mathrm{Al}}$ and be-

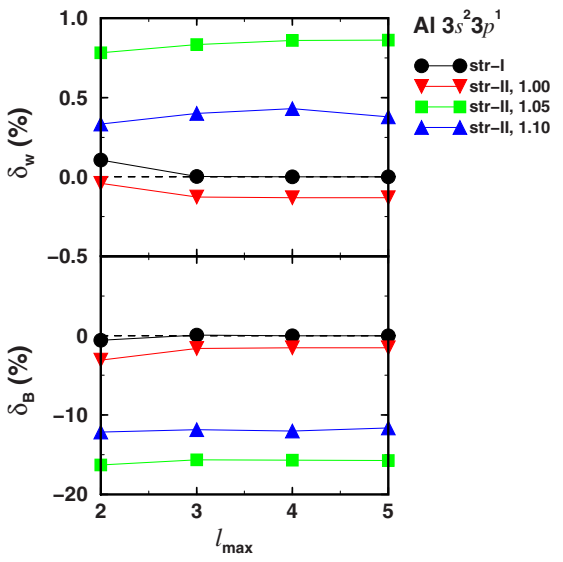

FIG. 2. (Color online) Relative errors of the LDA equilibrium WS radius and bulk modulus for Al ($3s^2 3p^1$) calculated for structure str-II as functions of the number of MT orbitals (l_{max}) and potential sphere radius ($1.00w^{\mathrm{II}}_{\mathrm{Al}}$, $1.05w^{\mathrm{II}}_{\mathrm{Al}}$, and $1.10w^{\mathrm{II}}_{\mathrm{Al}}$). See caption of Table II for the reference levels. Solid circles are the errors obtained for str-I Al.

TABLE II. Relative errors (in %) of the LDA equilibrium Wigner-Seitz radius (δ_w) and bulk modulus (δ_B) for Al ($3s^2 3p^1$) calculated for structure str-II as functions of l_{max} and S^{II}_{Al} (units of $\bar{w}^{II}_{Al}$). The errors are shown relative to w^{I}_{Al}=2.95 bohr and B^{I}_{Al}=81.2 GPa obtained for structure str-I using *spdfgh* basis (Table I).

	δ_w	δ_B	δ_w	δ_B	δ_w	δ_B	δ_w	δ_B
S^{II}_{Al}	*spd*		*spdf*		*spdfg*		*spdfgh*	
1.00	−0.04	−3.1	−0.13	−1.6	−0.13	−1.5	−0.13	−1.5
1.05	0.78	−16.3	0.84	−15.6	0.86	−15.7	0.86	−15.7
1.10	0.33	−12.2	0.40	−11.9	0.43	−12.0	0.38	−11.6

tween $B^{II}_{Al}(l_{max}, S^{II}_{Al})$ and B^{I}_{Al}. Here, w^{I}_{Al}=2.95 bohr and B^{I}_{Al}=81.2 GPa are the theoretical values obtained for structure str-I using the *spdfgh* basis (Table I). For comparison, in Fig. 2 the results obtained for structure str-I [i.e., the relative errors between $w^{I}_{Al}(l_{max})$ and w^{I}_{Al}, and between $B^{I}_{Al}(l_{max})$ and B^{I}_{Al}] are also shown.

We find that for Al there is no significant difference between the errors and their l_{max} dependence obtained for structures str-I and str-II. For all S^{II}_{Al} values, both w and B converge rapidly with l_{max}. In fact, for each potential sphere radius and for both structures we have $\delta_w \approx$ const. and $\delta_B \approx$ const. for $l_{max} \geq 2$. The excellent l_{max} convergence experienced for Al is a consequence of the well-localized core density (constrained within w^{II}_{Al}) and the nearly homogeneous valence density in this metal.

On the other hand, the potential sphere dependence of the relative errors turns out to be rather significant. For the Wigner-Seitz radius, excellent agreement is obtained between $w^{II}_{Al}(l_{max}, S^{II}_{Al})$ and w^{I}_{Al} for $S^{II}_{Al}=1.00\bar{w}^{II}_{Al}$. For the bulk modulus, the situation is also satisfactory: the error for $S^{II}_{Al}=1.00\bar{w}^{II}_{Al}$ is around −1.5%. Notice that no improvement is achieved by increasing the potential sphere radius to $1.05\bar{w}^{II}_{Al}$ and $1.10\bar{w}^{II}_{Al}$.

2. Copper

The relative errors for the equilibrium Wigner-Seitz radius and bulk modulus of Cu calculated for structure str-II are presented in Fig. 3 and Table III as functions of l_{max} and S^{II}_{Cu}. The notations and definitions are the same as for Al (Sec. III B 1). The results from Fig. 3 are markedly different from those presented for Al (in Fig. 2, notice the different scales). The change in δ_w for Al is close to zero compared to the largest change of 3.92% for Cu. The corresponding figures for δ_B are 1.6% for Al and 21.0% for Cu. Furthermore, for Al the errors are practically constant for $l_{max} \geq 2$ in contrast to Cu, where even the g and h orbitals have an impact on the equilibrium properties.

Comparing the errors for str-II to the errors for str-I from Fig. 3, we realize that whereas for the fcc Cu l_{max}=3 yields converged results, for str-II Cu at least l_{max}=4 (*spdfg*) is needed to stabilize δ_w and δ_B. We can conclude that, in spite of the fact that Cu has a nearly spherically symmetric density, it requires significantly more basis functions than Al

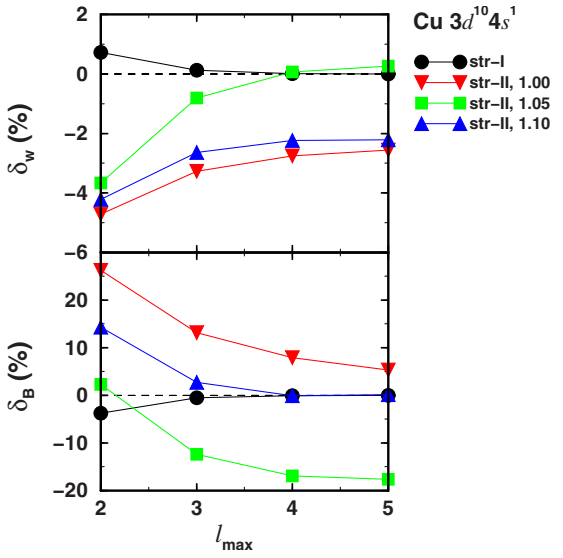

FIG. 3. (Color online) Relative errors of the LDA equilibrium WS radius and bulk modulus for Cu ($3d^{10}4s^1$) calculated for structure str-II as functions of the number of MT orbitals and potential sphere radius ($1.00\bar{w}^{II}_{Cu}$, $1.05\bar{w}^{II}_{Cu}$, and $1.10\bar{w}^{II}_{Cu}$). See caption of Table III for the reference levels. Solid circles are the errors obtained for str-I Cu.

when described in structure str-II. This behavior may be ascribed to the way how the spherical density around the Cu atoms is represented when expanded around the tetrahedral Em sites.

The potential sphere dependence of δ_w and δ_B for Cu is similar to that experienced for Al. It is found that $S^{II}_{Cu}=1.05\bar{w}^{II}_{Cu}$ yields accurate volume ($\delta_w < 0.3\%$ for *spdfg* and *spdfgh*). Unfortunately, this choice of S^{II}_{Cu} produces a large error in the bulk modulus of Cu ($|\delta_B| \approx 17\%$). Increasing S^{II}_{Cu} to $1.10\bar{w}^{II}_{Cu}$ decreases $|\delta_B|$ to 0.1% but increases $|\delta_w|$ to 2.21%, which is well above our target error bar of 0.5%. With the present setup, the optimal potential sphere for the Cu site in str-II Cu is estimated to be around $1.07\bar{w}^{II}_{Cu}$.

We speculate that the relatively large error for str-II Cu is due to the semicore states, which may give a nonspherical charge distribution around the tetrahedral sites. Therefore, we performed a few additional calculations for str-II Cu by treating this time the $3p$ semicore states as valance states (referred to as Cu*). The new set of results for $S^{II}_{Cu^*}$

TABLE III. Relative errors (in %) of the LDA equilibrium Wigner-Seitz radius (δ_w) and bulk modulus (δ_B) for Cu ($3d^{10}4s^1$) calculated for structure str-II as functions of l_{max} and S^{II}_{Cu} (units of $\bar{w}^{II}_{Cu}$). The errors are shown relative to w^{I}=2.60 bohr and B^{I}=185.7 GPa obtained for structure str-I using *spdfgh* basis (Table I).

	δ_w	δ_B	δ_w	δ_B	δ_w	δ_B	δ_w	δ_B
S^{II}_{Cu}	*spd*		*spdf*		*spdfg*		*spdfgh*	
1.00	−4.71	26.3	−3.27	13.1	−2.75	7.9	−2.55	5.3
1.05	−3.66	2.3	−0.81	−12.4	0.07	−16.9	0.26	−17.6
1.10	−4.21	14.3	−2.64	2.7	−2.23	−0.1	−2.21	0.1

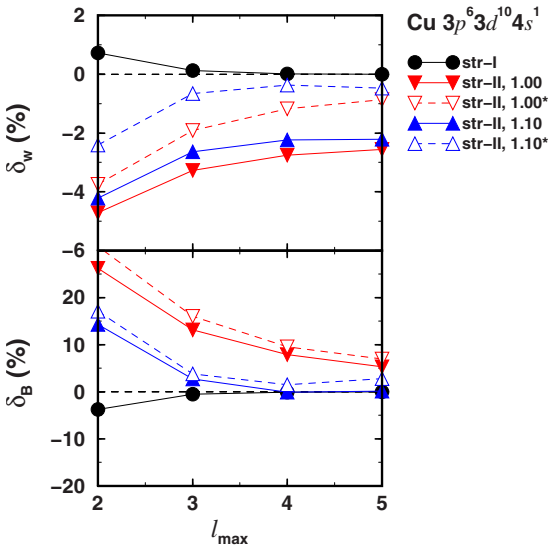

FIG. 4. (Color online) Relative errors of the LDA equilibrium WS radius and bulk modulus for Cu calculated for structure str-II as functions of the number of MT orbitals and potential sphere radius ($1.00\bar{w}^{\mathrm{II}}_{\mathrm{Cu}^*}$ and $1.10\bar{w}^{\mathrm{II}}_{\mathrm{Cu}^*}$). Notations: results with star (dashed lines) correspond to $3p^6 3d^{10} 4s^1$ configuration and those without star (solid lines) correspond to $3d^{10} 4s^1$ configurations. See caption of Table III for the reference levels. Solid circles are the errors obtained for str-I Cu.

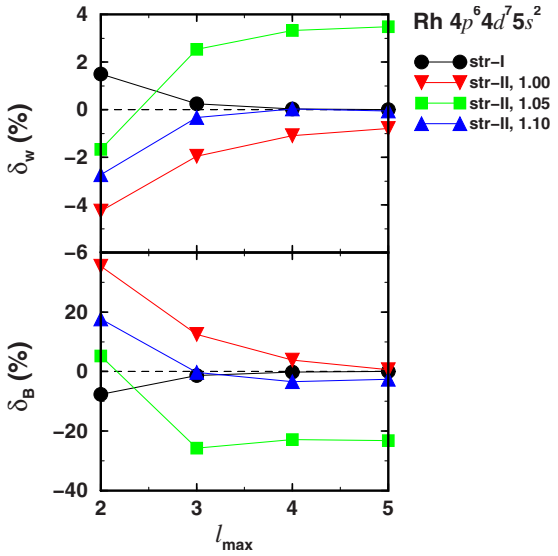

FIG. 5. (Color online) Relative errors of the LDA equilibrium WS radius and bulk modulus for Rh ($4p^6 4d^7 5s^2$) calculated for structure str-II as functions of the number of MT orbitals and potential sphere radius ($1.00\bar{w}^{\mathrm{II}}_{\mathrm{Rh}}$, $1.05\bar{w}^{\mathrm{II}}_{\mathrm{Rh}}$, and $1.10\bar{w}^{\mathrm{II}}_{\mathrm{Rh}}$). See caption of Table IV for the reference levels. Solid circles are the errors obtained for str-I Rh.

$=1.00\bar{w}^{\mathrm{II}}_{\mathrm{Cu}^*}$ and $1.10\bar{w}^{\mathrm{II}}_{\mathrm{Cu}^*}$ are displayed in Fig. 4 as a function of l_{max} (dashed lines). For comparison, the corresponding values obtained for str-I Cu and for str-II Cu having the $3p$ states in the core (Fig. 3) are also shown (solid lines). We observe that by placing the $3p$ states into the valence, the relative error for the Wigner-Seitz radius decreases by $\sim 2\%$. At the same time, for the bulk modulus the two sets of data agree quite well with each other. These two effects altogether lead to much a better equation of state for str-II Cu^* with $3p$ states in the valance than that with $3p$ states in the core. In particular, for $S^{\mathrm{II}}_{\mathrm{Cu}^*}=1.10\bar{w}^{\mathrm{II}}_{\mathrm{Cu}^*}$ and $l_{max}\geq 4$, the new relative errors become $|\delta_w|<0.48$ and $|\delta_B|\leq 2.8$. These errors are in fact close to the error bars of our calculations. It is clear that when describing interstitial positions in close-packed systems a special care must be taken of the semicore states as they may significantly influence the calculated results.

3. Rhodium

The slow basis convergence seen for str-II Cu is expected to be even worse for str-II Rh. Indeed, as shown in Fig. 5 and Table IV, for Rh the largest changes in δ_w and δ_B versus l_{max} are 5.15% and 34.8%, respectively, compared to 3.92% and 21.0% found for Cu. To make the difference between Cu and Rh clearer, we compare the relative errors obtained for $S^{\mathrm{II}}=1.00\bar{w}^{\mathrm{II}}$ using *spdf* and *spdfgh* bases. For $|\delta_w(spdfgh)-\delta_w(spdf)|$, we get 0.72% for Cu and 1.17% for Rh (0.00% for Al). The corresponding numbers for $|\delta_B(spdfgh)-\delta_B(spdf)|$ are 7.8% and 11.9%, respectively (0.1% for Al). Repeating the comparison for the errors obtained using *spdfg* and *spdfgh*, the error differences for w and B drop to 0.20% and 1.7% for Cu, and 0.31% and 3.3% for Rh, respectively. This clearly demonstrates that in str-II structure the basis convergence for Rh is slower compared to that for Cu, and in general the two transition metals require a significantly larger basis set than Al.

To understand the above trend, we compare the charge distributions in Rh and Cu. In addition to the more localized d states present in both metals, fcc Rh has somewhat larger interstitial density compared to Cu, which makes the charge flow into the tetrahedral Em spheres more pronounced. Furthermore, the $4p$ semicore states of Rh are located relatively close to the valence states. Depending on the size of the potential spheres on the Rh site ($S^{\mathrm{II}}_{\mathrm{Rh}}$), these semicore states might penetrate into the tetrahedral Em potential spheres. According to our atomic calculations, in Rh approximately 0.13 electrons ($\sim 2\%$ of the $4p$ electrons) are located outside the sphere of radius $\bar{w}^{\mathrm{II}}_{\mathrm{Rh}}$. For comparison, in the case of Cu $\sim 99\%$ of the $3p$ electrons and for Al all $2p$ electrons are constrained within their Wigner-Seitz spheres. The large interstitial density and the semicore charge leakage in Rh are

TABLE IV. Relative errors (in %) of the LDA equilibrium Wigner-Seitz radius (δ_w) and bulk modulus (δ_B) for Rh ($4p^6 4d^7 5s^2$) calculated for structure str-II as functions of l_{max} and $S^{\mathrm{II}}_{\mathrm{Rh}}$ (units of $\bar{w}^{\mathrm{II}}_{\mathrm{Rh}}$). The errors are shown relative to $w^{\mathrm{I}}=2.78$ bohr and $B^{\mathrm{I}}=313.9$ GPa obtained for structure str-I using *spdfgh* basis (Table I).

	δ_w	δ_B	δ_w	δ_B	δ_w	δ_B	δ_w	δ_B
$S^{\mathrm{II}}_{\mathrm{Rh}}$	*spd*		*spdf*		*spdfg*		*spdfgh*	
1.00	−4.25	35.4	−1.96	12.5	−1.10	3.9	−0.79	0.6
1.05	−1.67	5.2	2.53	−25.7	3.33	−22.9	3.48	−23.2
1.10	−2.73	17.6	−0.33	−0.4	0.04	−3.5	−0.06	−2.6

TABLE V. Theoretical equilibrium Wigner-Seitz radii (in bohr) and total energies (in Ry) for Sc, ScH, and ScH_2 calculated using the EMTO and VASP methods and the PBE exchange-correlation approximation. The crystal structures (strukturbericht designations) are shown in the second column. The total energies and the Wigner-Seitz radii for ScH and ScH_2 are given relative to those for pure fcc Sc. The EMTO results are listed for $l_{max}=2$, 3, 4, and 5 and they correspond to $S^{II}_{Sc}=1.00\bar{w}^{II}_{Sc}$.

		EMTO								VASP	
		spd		*spdf*		*spdfg*		*spdfgh*			
	Str.	w_{II}	ΔE	w_{II}	ΔE	w_{II}	ΔE	w_{II}	ΔE	w_I	ΔE
Sc	A1	3.316		3.374		3.389		3.395		3.405	
ScH	B3	0.164	−1.225	0.121	−1.230	0.113	−1.231	0.109	−1.232	0.096	−1.233
ScH_2	$C1_2$	0.197	−2.472	0.146	−2.480	0.135	−2.482	0.131	−2.482	0.103	−2.479

also reflected by the multipole moments around the tetrahedral Em sites from the str-II structures. For instance, the calculated charge density moments for $l=3$ and $m=-2$ are 0.002, 0.027, and 0.062 electrons, for Al, Cu, and Rh, respectively. Thus, there is a strongly inhomogeneous charge density around the tetrahedral Em sites in str-II Rh, which explains the slow basis convergence experienced for this system.

The potential sphere dependence of the ground-state parameters of Rh follows a similar trend as that for Al and Cu. Both errors are relatively small for $S^{II}_{Rh}=1.00\bar{w}^{II}_{Rh}$ and $l_{max}=5$. However, the best result is found for $S^{II}_{Rh}=1.10\bar{w}^{II}_{Rh}$, where the relative errors for $l_{max}\geq 4$ are $|\delta_w|<0.06$ and $|\delta_B|\leq 3.5$. We point out that the above choice for S^{II}_{Rh} and $l_{max}=5$ gives a rather accurate description of the bulk properties of Rh in the str-II structure.

IV. APPLICATION TO HYDROGENATED Sc-BASED ALLOYS

The hydrogen absorption in $ScAl_{0.8}Mg_{0.2}$ was recently studied by Sahlberg *et al.*[45] using *in situ* synchrotron radiation powder x-ray diffraction, neutron powder diffraction, as well as first-principles quantum-mechanical calculations. Details about the calculations and theoretical results can be found in Ref. 45. Here, we focus on some important issues that were not considered before.

According to the experiment,[45] $ScAl_{0.8}Mg_{0.2}$ crystallizes in CsCl (B1), with Sc on the 1*a* site and random $Al_{0.8}Mg_{0.2}$ alloy on the 1*b* site. Upon hydrogen absorption at 10 MPa pressure and 400 °C, $ScAl_{0.8}Mg_{0.2}$ decomposes into ScH_2 with fluorite structure and fcc $Al_{0.8}Mg_{0.2}$. In order to assess the performance of our computational tool for the hydrogenation of Sc-based alloys, we first investigate the hydrogen reaction with pure Sc. For the beginning, we consider Sc in fcc structure, ScH_2 in CaF_2 structure, and ScH in ZnS structure, with the latter modeling the 50% hydrogen occupancy in the CaF_2 structure. All these three systems can be described using the lattice model from Fig. 1 with Em potential well on the octahedral site. For fcc Sc both tetrahedral sites are occupied by Em wells. For ScH one tetrahedral site is occupied by H and the other by Em. Finally, for ScH_2 both tetrahedral sites are occupied by H. For this study, in addition to the EMTO method, we also employed the Vienna *ab initio* simulation package (VASP),[52] which is based on the projector augmented wave method and it is a highly accurate full-potential tool. The VASP results presented in this section are considered to be well-converged values with respect to the energy cutoff and Brillouin-zone sampling. Thus, by comparing the EMTO results with those obtained using the VASP one can establish the accuracy of the muffin-tin approach for the fcc, ZnS, and CaF_2 structures.

Table V displays the basis set convergence of the Wigner-Seitz radius for str-II Sc calculated using the EMTO method with $l_{max}=2$, 3, 4, and 5. Compared to $w^{I}_{Sc}=3.411$ bohr, obtained for str-I Sc using the EMTO method, the relative error in the equilibrium radius of Sc decreases from −2.79% to −0.47% as going from the *spd* to *spdfgh* basis set. This trend is similar to the one obtained for Rh (Table IV). As a matter of fact, the *spdfgh* w^{II}_{Sc} agrees rather well with the VASP value of 3.405 bohr.

According to the VASP results, hydrogen addition to fcc Sc increases the equilibrium Wigner-Seitz radius by 0.095 bohr in ScH and by 0.103 bohr in ScH_2. Using the EMTO method with the *spd* basis, for the above lattice expansions we obtain 0.164 and 0.197 bohr, corresponding to 73% and 91% errors, respectively. Increasing the *l* cutoff to $l_{max}=5$ decreases the deviation between the VASP and EMTO lattice expansions to 15% for ScH and 27% for ScH_2. This is a significant improvement and clearly demonstrates that an accurate volume effect upon hydrogenation can only be obtained if a sufficiently large basis set is involved in the muffin-tin method.

The total-energy differences from Table V show somewhat better convergence with l_{max} than the Wigner-Seitz radius. Already with the *spdf* basis the energies are converged within 2 mRy. The deviations between the best EMTO (obtained for $l_{max}=5$) and the VASP relative energies are ~1 mRy for ScH and ~3 mRy for ScH_2. These differences are reasonable especially if we take into account that both methods have numerical uncertainties.

The chemical reaction between the hexagonal close-packed (hcp) Sc and hydrogen gas, viz.,

$$\mathrm{Sc(hcp)} + \mathrm{H_2(gas)} \rightarrow \mathrm{ScH_2(CaF_2)} \qquad (1)$$

is exothermic if the Gibbs energy of scandium dihydride is below the Gibbs energy of pure Sc plus the Gibbs energy of hydrogen. The latter is calculated according to[53]

$$G_{H_2}(T) = E_{H_2} + k_B T\left[\ln\left(\frac{p_{H_2}}{k_B T n_Q}\right) - \ln Z_{int}\right],$$

where $E(H_2)=-2.345$ Ry is the theoretical (generalized gradient level) total energy of a H_2 molecule,[54] p_{H_2} is the pressure of the H_2 gas, the quantum concentration is $n_Q=(mk_BT/2\pi\hbar^2)^{3/2}$ (m stands for the mass of a H_2 molecule, $\hbar$ is the Planck constant, and k_B is the Boltzmann constant), and Z_{int} is the partition function of the internal states due to the rotational and vibrational degrees of freedom. Assuming that the temperature-dependent terms in the Gibbs energies for the two solids in reaction (1) are similar, for the EMTO Gibbs energy of the reaction, we obtain $\Delta G_{Sc}(T)\approx -2.486$ Ry$-G_{H_2}(T)$. In this expression the fcc-hcp energy difference for Sc (4.0 mRy) has been added to the *spdfgh* relative energy from Table V. Using the expression for $G_{H_2}(T)$, we find that at $p_{H_2}=1$ atm hydrogen pressure, reaction (1) remains exothermic up to ~1286 K. The VASP energies yield a very similar critical temperature (1279 K). Our theoretical prediction is in good agreement with the experimental observation, namely, that ScH_2 does not desorb hydrogen below ~1230 K.[56]

Next we consider the hydrogenation of $ScAl_{0.8}Mg_{0.2}$ having the CsCl crystal structure, viz.,

$$ScAl_{0.8}Mg_{0.2}(CsCl) + H_2(gas) \rightarrow Sc_{0.5}Al_{0.4}Mg_{0.1}H_2(CaF_2). \quad (2)$$

The total energies for the two solids in reaction (2) have been determined using the EMTO method in combination with the coherent potential approximation.[14,15] In these calculations, random distribution was assumed for Al and Mg on the 1*b* site of the CsCl structure and for Sc, Al, and Mg on the 4*a* site of the CaF_2 structure. The calculated total energies (not shown) for the Gibbs energy of reaction (2) yield $\Delta G_{alloy}(T)\approx -2.338$ Ry$-G_{H_2}(T)$. Thus, we obtain that reaction (2) is endothermic for any T. We should note, however, that a slightly different *ab initio* total energy for the hydrogen molecule[55] predicts exothermic reaction below ~100 K. We can conclude that the stability field of ScH_2 is substantially reduced by adding 40% Al and 10% Mg to Sc. The preferential formation of $ScAl_{0.8}Mg_{0.2}$ and the presence of Al and Mg in $Sc_{0.5}Al_{0.4}Mg_{0.1}H_2$ strongly destabilized the hydrogenation reaction (2). This result is fully supported by experiment.[45] Furthermore, the facts that ScH_2 can easily form even at elevated temperatures and $Sc_{0.5}Al_{0.4}Mg_{0.1}H_2$ is unstable already at zero temperature suggest that the hydrogen adsorption drives the $ScH_2+Al_{0.8}Mg_{0.2}$ phase separation observed in hydrogenated $ScAl_{0.8}Mg_{0.2}$.[45]

V. CONCLUSIONS

We have investigated the basis set convergence of the exact muffin-tin orbitals by calculating the equation of state for Al, Cu, and Rh in two equivalent crystal lattices: first is the conventional face-centered-cubic lattice (str-I) and the second is a face-centered-cubic lattice with one atomic and three empty sites per primitive cell (str-II). For the fcc lattice, the *spd* basis for Al and the *spdf* basis for Cu and Rh yield well-converged equilibrium properties. We have demonstrated that Al is well described by the *spd* basis also in structure str-II. On the other hand, for str-II Cu and Rh at least five orbitals (*spdfg*) are needed to get converged equilibrium Wigner-Seitz radius (within $\lesssim$0.3%) and bulk modulus ($\lesssim$3.3%). The slow basis convergence for these two systems has been ascribed to the spherical densities and the semicore states around the atomic sites. These densities penetrate the tetrahedral Em spheres from structure str-II, creating there a strongly inhomogeneous (nonsymmetric) charge distribution.

The muffin-tin potential sphere radius dependence of the calculated bulk properties for structures str-II has also been discussed. We have found that for Al $S^{II}_{Al}=1.00\bar{w}^{II}_{Al}$ and for Rh $S^{II}_{Rh}=1.10\bar{w}^{II}_{Rh}$ ensure a very good representation of the full potential. For Cu with 3*p* states in the core, the best potential sphere radius is estimated to be around $1.07\bar{w}^{II}_{Cu}$. Nevertheless, when the 3*p* states are treated as valence states, $S^{II}_{Cu^*}=1.10\bar{w}^{II}_{Cu^*}$ yields bulk properties in good agreement with those obtained for the fcc lattice.

The basis set convergence within the EMTO method has been demonstrated on hydrogenated Sc and Sc-based alloys. The present results indicate that while ScH_2 remains stable up to ~1300 K (at ambient pressure) against hydrogen desorption, Al and Mg additions to Sc strongly destabilize the hydrogenated alloy and lead to the experimentally observed $ScH_2+Al_{0.8}Mg_{0.2}$ phase separation. The EMTO method has been found to be a particularly useful tool to study the chemical reaction of hydrogen with $ScAl_{0.8}Mg_{0.2}$ since it can properly account for both the chemical disorder and the interstitial hydrogen in the fcc structure.

Our results clearly demonstrate that the accuracy of the MT methods can be sustained at a reasonably high level even in the case of low-symmetry structures. In applications based on the EMTO approach, however, special emphasis should be put on the completeness of the basis set and on the choice of the size of the potential spheres.

ACKNOWLEDGMENTS

The Swedish Research Council, the Swedish Foundation for Strategic Research, the Swedish Energy Agency, the Carl Tryggers Foundation, the Erasmus Mundus External Cooperation Window Lot3, and the Hungarian Scientific Research Fund (Contract No. T048827) are acknowledged for financial support.

[1] P. Hohenberg and W. Kohn, Phys. Rev. **136**, B864 (1964).
[2] W. Kohn and L. J. Sham, Phys. Rev. **140**, A1133 (1965).
[3] J. Korringa, Physica (Amsterdam) **13**, 392 (1947).
[4] W. Kohn and N. Rostoker, Phys. Rev. **94**, 1111 (1954).
[5] L. Szunyogh, B. Ujfalussy, P. Weinberger, and J. Kollár, Phys. Rev. B **49**, 2721 (1994).
[6] H. L. Skriver, *The LMTO Method* (Springer-Verlag, Berlin, 1984).
[7] O. K. Andersen, O. Jepsen, and M. Sob, in *Linearized Band Structure Methods*, Lecture Notes in Physics: Electronic Band Structure and Its Applications, edited by M. Yussouff (Springer-Verlag, Berlin, 1987).
[8] J. Kübler, *Theory of Itinerant Electron Magnetism* (Clarendon Press, Oxford, 2000).
[9] O. K. Andersen, A. V. Postnikov, and S. Y. Savrasov, in *Applications of Multiple Scattering Theory in Materials Science*, edited by W. H. Butler, P. H. Dederichs, A. Gonis, and R. L. Weaver (Materials Research Society, Pittsburgh, PA, 1992).
[10] O. K. Andersen, O. Jepsen, and G. Krier, *Lectures on Methods of Electronic Structure Calculation* (World Scientific, Singapore, 1994), p. 63.
[11] O. K. Andersen, C. Arcangeli, R. W. Tank, T. Saha-Dasgupta, G. Krier, O. Jepsen, and I. Dasgupta, *Tight-Binding Approach to Computational Materials Science*, edited by L. Colombo, A. Gonis, and P. Turchi, MRS Symposia Proceedings No. 91 (Materials Research Society, Pittsburgh, PA, 1998), p. 3–34.
[12] L. Vitos, H. L. Skriver, B. Johansson, and J. Kollár, Comput. Mater. Sci. **18**, 24 (2000).
[13] L. Vitos, Phys. Rev. B **64**, 014107 (2001).
[14] L. Vitos, I. A. Abrikosov, and B. Johansson, Phys. Rev. Lett. **87**, 156401 (2001).
[15] L. Vitos, *The EMTO Method and Applications*, Computational Quantum Mechanics for Materials Engineers (Springer-Verlag, London, 2007).
[16] J. M. Wills, O. Eriksson, M. Alouani, and D. L. Price, in *Electronic Structure and Physical Properties of Solids: The Uses of the LMTO Method*, Lecture Notes in Physics, edited by H. Dreyssé (Springer-Verlag, Berlin, 2000), p. 148.
[17] M. Methfessel, M. van Schilfgaarde, and R. A. Casali, in *Electronic Structure and Physical Properties of Solids: The Uses of the LMTO Method*, Lecture Notes in Physics, edited by H. Dreyssé (Springer-Verlag, Berlin, 2000), p. 114.
[18] S. Y. Savrasov and D. Y. Savrasov, Phys. Rev. B **54**, 16487 (1996).
[19] M. Asato, A. Settels, T. Hoshino, T. Asada, S. Blügel, R. Zeller, and P. H. Dederichs, Phys. Rev. B **60**, 5202 (1999).
[20] V. L. Moruzzi, J. F. Janak, and A. R. Williams, *Calculated Electronic Properties of Metals* (Pergamon, New York, 1978).
[21] V. L. Moruzzi, J. F. Janak, and K. Schwarz, Phys. Rev. B **37**, 790 (1988).
[22] H. L. Skriver, Phys. Rev. B **31**, 1909 (1985).
[23] L. Vitos, J. Kollár, and H. L. Skriver, Phys. Rev. B **55**, 13521 (1997).
[24] J. Kollár, L. Vitos, and H. L. Skriver, in *Electronic Structure and Physical Properties of Solids: The Uses of the LMTO Method*, Lecture Notes in Physics, edited by H. Dreyssé (Springer-Verlag, Berlin, 2000), p. 85.
[25] P. Olsson, I. A. Abrikosov, L. Vitos, and J. Wallenius, J. Nucl. Mater. **321**, 84 (2003).
[26] L. Dubrovinsky, N. Dubrovinskaia, F. Langenhorst, D. Dobson, D. Rubie, C. Geβmann, I. A. Abrikosov, B. Johansson, V. I. Baykov, L. Vitos, T. Le Bihan, W. A. Crichton, V. Dmitriev, and H.-P. Weber, Nature (London) **422**, 58 (2003).
[27] L. Vitos, P. A. Korzhavyi, and B. Johansson, Phys. Rev. Lett. **96**, 117210 (2006).
[28] N. Dubrovinskaia, L. Dubrovinsky, I. Kantor, W. A. Crichton, V. Dmitriev, V. Prakapenka, G. Shen, L. Vitos, R. Ahuja, B. Johansson, and I. A. Abrikosov, Phys. Rev. Lett. **95**, 245502 (2005).
[29] A. Taga, L. Vitos, B. Johansson, and G. Grimvall, Phys. Rev. B **71**, 014201 (2005).
[30] L. Huang, L. Vitos, S. K. Kwon, B. Johansson, and R. Ahuja, Phys. Rev. B **73**, 104203 (2006).
[31] J. Zander, R. Sandström, and L. Vitos, Comput. Mater. Sci. **41**, 86 (2007).
[32] A. E. Kissavos, S. I. Simak, P. Olsson, L. Vitos, and I. A. Abrikosov, Comput. Mater. Sci. **35**, 1 (2006).
[33] L. Vitos, P. A. Korzhavyi, and B. Johansson, Nature Mater. **2**, 25 (2003).
[34] B. Magyari-Köpe, G. Grimvall, and L. Vitos, Phys. Rev. B **66**, 064210 (2002); **66**, 179902(E) (2002).
[35] B. Magyari-Köpe, L. Vitos, and G. Grimvall, Phys. Rev. B **70**, 052102 (2004).
[36] L. Vitos, P. A. Korzhavyi, and B. Johansson, Phys. Rev. Lett. **88**, 155501 (2002).
[37] B. Magyari-Köpe, L. Vitos, B. Johansson, and J. Kollár, J. Geophys. Res. **107**, 2136 (2002).
[38] A. Landa, C.-C. Chang, P. N. Kumta, L. Vitos, and I. A. Abrikosov, Solid State Ionics **149**, 209 (2002).
[39] B. Magyari-Köpe, L. Vitos, G. Grimvall, B. Johansson, and J. Kollár, Phys. Rev. B **65**, 193107 (2002).
[40] B. Magyari-Köpe, L. Vitos, B. Johansson, and J. Kollár, Acta Crystallogr., Sect. B: Struct. Sci. **57**, 491 (2001).
[41] L. Vitos, J. Kollár, and H. L. Skriver, Phys. Rev. B **49**, 16694 (1994).
[42] J. Kollár, L. Vitos, and H. L. Skriver, Phys. Rev. B **49**, 11288 (1994).
[43] M. Zwierzycki and O. K. Andersen, Acta Phys. Pol. A **115**, 64 (2009).
[44] M. Ropo, K. Kokko, and L. Vitos, Phys. Rev. B **77**, 195445 (2008).
[45] M. Sahlberg, P. Beran, T. K. Nielsen, Y. Cerenius, K. Kádas, M. P. J. Punkkinen, L. Vitos, O. Eriksson, T. R. Jensen, and Y. Andersson, J. Solid State Chem. **182**, 3113 (2009).
[46] J. P. Perdew and Y. Wang, Phys. Rev. B **45**, 13244 (1992).
[47] D. M. Ceperley and B. J. Alder, Phys. Rev. Lett. **45**, 566 (1980).
[48] J. P. Perdew, A. Ruzsinszky, G. I. Csonka, O. A. Vydrov, G. E. Scuseria, L. A. Constantin, X. Zhou, and K. Burke, Phys. Rev. Lett. **100**, 136406 (2008); see also the supplementary information.
[49] J. P. Perdew, K. Burke, and M. Ernzerhof, Phys. Rev. Lett. **77**, 3865 (1996).
[50] A. E. Kissavos, L. Vitos, and I. A. Abrikosov, Phys. Rev. B **75**, 115117 (2007).
[51] D. A. Young, *Phase Diagrams of the Elements* (University of California Press, Berkeley, CA, 1991).
[52] G. Kresse and J. Hafner, Phys. Rev. B **47**, 558 (1993); **49**, 14251 (1994); G. Kresse and J. Furthmüller, Comput. Mater. Sci. **6**, 15 (1996); Phys. Rev. B **54**, 11169 (1996).

[53] C. G. Van de Walle and J. Neugebauer, Phys. Rev. Lett. **88**, 066103 (2002).
[54] K. G. Nakamura, K. Ishioka, M. Kitajima, A. Endou, M. Kubo, and A. Miyamoto, J. Chem. Phys. **108**, 3222 (1998).
[55] S. Kurth, J. P. Perdew, and P. Blaha, Int. J. Quantum Chem. **75**, 889 (1999).
[56] A. G. Aleksanyan, S. K. Dolukhanyan, V. S. Shekhtman, K. S. Harutyunyan, K. A. Abrahamyan, and N. L. Mnatsakanyan, J. Alloys Compd. **356-357**, 562 (2003).